Transition behavior of the discrete nonlinear Schrödinger equation

Benno Rumpf
Institute of Physics, Chemnitz University of Technology, 09107 Chemnitz, Germany
(Received 9 November 2007; published 10 March 2008)

Many nonlinear lattice systems exhibit high-amplitude localized structures, or discrete breathers. Such structures emerge in the discrete nonlinear Schrödinger equation when the energy is above a critical threshold. This paper studies the statistical mechanics at the transition and constructs the probability distribution in the regime where breathers emerge. The entropy as a function of the energy is nonanalytic at the transition. The entropy is independent of the energy in the regime of breathers above the transition.

DOI: 10.1103/PhysRevE.77.036606 PACS number(s): 05.45.Yv, 63.20.Pw, 63.70.+h

I. INTRODUCTION

Localized high-amplitude structures, or discrete breathers, are observed in such diverse discrete nonlinear systems as microcantilevers [1], networks of Josephson junctions [2], in molecular dynamics [3], crystal lattice vibrations [4], and in antiferromagnetic spin wave dynamics [5]. It is a question both of practical and of fundamental interest why energy is persistently stored by localized nonlinear modes of spatially discrete systems.

An important example of an equation of motion with breather solutions is the discrete nonlinear Schrödinger equation

$$i\dot{\phi}_n = J(\phi_{n+1} + \phi_{n-1}) + |\phi_n|^2\phi_n. \tag{1}$$

This equation has important applications in coupled optical waveguides [6] and in the dynamics of Bose-Einstein condensates trapped in periodic potentials [7]. The discrete nonlinear Schrödinger equation derives as $i\dot{\phi}_n = \partial E/\partial\phi_n^*$ from the Hamiltonian $E = E_2 + E_4 = \Sigma_n J\phi_n^*(\phi_{n+1} + \phi_{n-1}) + \frac{1}{2}\Sigma_n\phi_n^2\phi_n^{*2}$. The wave action $A = \Sigma_n|\phi_n|^2$ is a second conserved quantity, which is due to the phase symmetry of Eq. (1).

The dynamics of Eq. (1) is radically different in two regimes that depend on the two conserved quantities E and A. Figure 1(a) shows the probability density function and a snapshot of $|\phi_n|^2$ in the regime where breathers do emerge. The initial condition for the simulation is almost homogeneous in space, with low amplitudes $\phi_n \approx 0.3$. A few localized high-amplitude breathers emerge during the time evolution. These peaks are inert for any achievable long-time simulation. The peaks appear as a hump in the probability density function $p(|\phi|^2)$ at $|\phi|^2 \approx 4.5$. Most of the probability, however, is at low amplitudes $|\phi|^2 \ll 1$, corresponding to disordered low-amplitude waves.

Figure 1(b) shows data for the regime where no breathers emerge. The initial condition is a low-amplitude wave with a wave number $k = \pi/2$. This corresponds to a lower energy E than Fig. 1(a). A state of disordered low-amplitude waves with no high-amplitude peaks develops from this initial condition. The probability density function decays as $\ln p(|\phi|^2) \sim -|\phi|^2$ at all lattice sites, with no hump at higher amplitudes.

Recent studies have shown that discrete breathers are part of the state of maximum entropy of the discrete nonlinear Schrödinger equation and other lattices where a second quantity is conserved in addition to the Hamiltonian [8–11]. Both the regime with breathers and the regime with no breathers can be explained with this statistical approach.

The transition from the regime with no breathers to the breather regime has been attributed to a change of the sign of the system's temperature [8]. For the grand canonical distribution function $p \sim \exp(-\epsilon E - \alpha A)$, the transition line $\epsilon = 0$ is

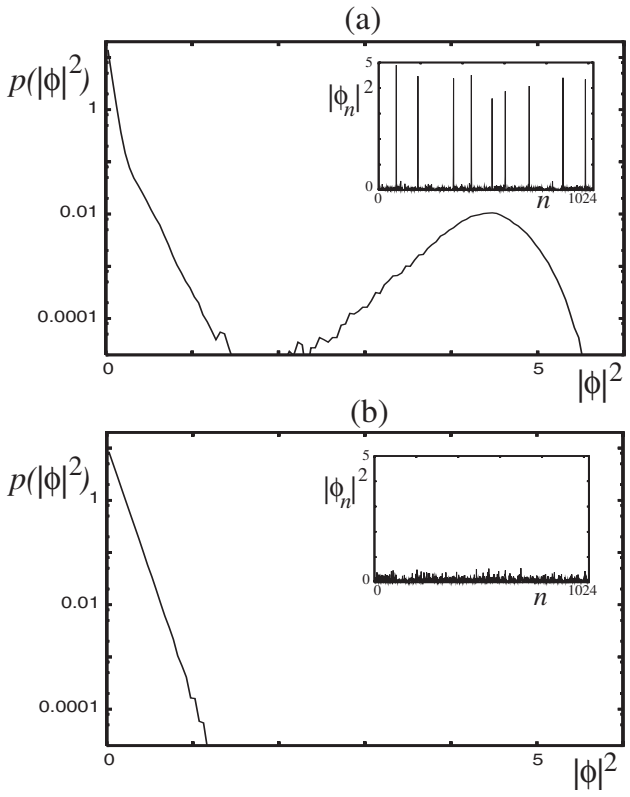

FIG. 1. Numerical results for the discrete nonlinear Schrödinger equation of $N = 1024$ oscillators with periodic boundary conditions. The coupling constant is $J = 1$. $p(|\phi|^2)$ is the probability density function averaged over time and over the lattice sites. The insets show snapshots of $|\phi_n|^2$ after an integration of 50 000 time units. (a) High-amplitude peaks with $|\phi_n|^2 \approx 4.5$ emerge from a low-amplitude background for the initial condition $\phi_n = 0.3$ plus weak noise. The probability density has a hump at high amplitudes that is due to these peaks. (b) No peaks emerge for the initial condition $\phi_n = 0.3\exp(i\pi n/2)$ plus weak noise. The probability density function decays exponentially.

given by $E=A^2/N$. The energy in the simulation of Fig. 1(b) is slightly below this threshold. An energy below the threshold corresponds to $\epsilon>0$ so that the grand canonical density decays rapidly as a function of $|\phi_n|$. The probability for high amplitude excitations $|\phi_n|^2 \gg 1$ is extremely low.

The simulation of Fig. 1(a) with breathers corresponds to an energy $E>A^2/N$ above the threshold. The problem with the statistical description of this regime is that no grand canonical distribution yields a finite energy $E>A^2/N$. In particular, the grand canonical density diverges at high $|\phi_n|$ when ϵ is negative.

References [9,10] address the statistics in the breather regime with a fixed energy and wave action. The high-amplitude breathers and the low-amplitude phonon waves are considered as two interacting thermodynamic systems. Most of the entropy is due to the phonons, and very little entropy is due to the breathers. The system's entropy is maximal if the right amount of energy is allocated to the phonons. Breathers emerge when the total energy is above the amount that is required by the phonons. This surplus of energy gathers in discrete breathers. This mechanism is widespread in systems with two conserved quantities [9].

A number of studies [12,13] concern ensembles that are canonical in the energy and microcanonical in the wave action. This corresponds to a system that is coupled to a heat bath with a fixed temperature, from which it can draw an infinite amount of energy [12,14]. Study spatially continuous nonlinear Schrödinger systems, where the entropy is dominated by the degrees of freedom at infinitesimal length scales. The state of maximum entropy for a fixed energy and wave action corresponds to a macroscopic soliton structure and fluctuations with an infinitesimal amplitude and with infinitesimal wavelengths [14].

This paper is devoted to the transition behavior between the two regimes and to the regime where breathers exist. Energy and wave action are set by the initial conditions and conserved. The probability distribution is derived from the extremum of entropy with the constraints of fixed energy and wave action. A simplified discrete nonlinear Schrödinger Eq. (1) with a weak coupling force $J \ll 1$ is studied in Sec. II. These results are extended to the system with a finite coupling strength in Sec. III.

II. ENTROPY IN THE WEAK-COUPLING LIMIT

A. Energy and wave action for weakly coupled oscillators

In this section, Eq. (1) is studied in the limit of weak coupling $J \ll 1$. Each oscillator is predominantly governed by the nonlinear part $i\dot{\phi}_n \approx \phi_n|\phi_n|^2$. Most of the energy $E \approx E_4$ is stored in the quartic part of the Hamiltonian, whereas the coupling term $E_2 \sim O(J)$ contains only a negligible amount of energy. The trajectory is confined to the shell of constant $E \approx E_4$ and A in phase space.

The weak coupling allows the system to thermalize on this shell. Each oscillator can transfer energy and wave action to the other oscillators, or can receive these quantities. Correlations between the oscillators are expected to vanish in the limit of small coupling. The probability density

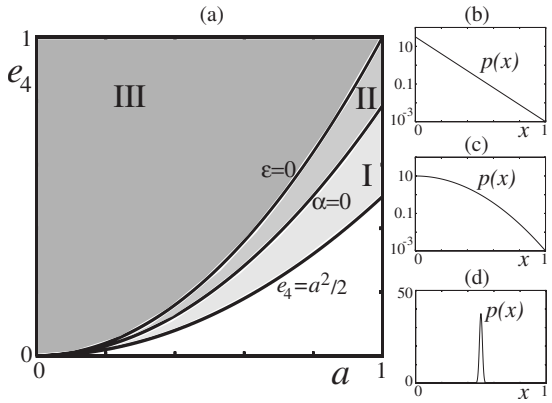

FIG. 2. (a) Domains I and II with no breathers and domain III with breathers in the a-e_4 diagram for a single oscillator. The domains are separated by the line $e_4=a^2$ with $\epsilon=0$, and $e_4=\pi a^2/4$ with $\alpha=0$. The lowest possible energy is $e_4=a^2/2$. Domain I corresponds to $\alpha<0$, $\epsilon>0$, domain II to $\alpha>0$, $\epsilon>0$. (b) $\ln p(x) = \ln \alpha - \alpha x$ at line $\epsilon=0$. (c) $\ln p(x)=\ln\sqrt{4\epsilon/\pi-\epsilon x^2/2}$ at line $\alpha=0$. (d) Peaked density at $\epsilon=-\alpha \gg 1$ at the minimum of energy $e_4 = a^2/2$.

$p_N(\phi_1, \phi_2, \ldots, \phi_N)=\Pi_{n=1}^N p_1(\phi_n)$ factorizes into a product of densities of the single oscillators ϕ_n. Each oscillator is described by the same probability density function p_1.

The Hamiltonian E_4 is invariant under the transformation $\phi_n \to \phi_n \exp(i\alpha_n)$. Exploiting this phase symmetry, it is convenient to describe the oscillator ϕ_n by one radial variable $x_n=\pi|\phi_n|^2 \geq 0$. A phase space volume element is given by $dx_n=\pi d|\phi_n|^2$. This leads to the probability density $p(x)$ with the normalization $\int_0^\infty p(x)dx=1$ on a real sample space $x \geq 0$. This probability density applies to each single oscillator.

The average wave action per oscillator $a=A/N = \pi^{-1}\int_0^\infty p(x)xdx=\langle x\rangle/\pi$ is proportional to the first moment. The average energy $e_4=E_4/N=2^{-1}\pi^{-2}\int_0^\infty p(x)x^2dx = \langle x^2\rangle/(2\pi^2)$ is proportional to the second moment.

The range of possible energies at a given wave action a is bounded from below and unbounded from above. The lowest possible energy $e_4(a)=a^2/2$ is achieved for the density $p(x)=\delta(x-a\pi)$ (Fig. 2). There is no upper limit of the energy: For instance, the density $p(x)=(1-c)\delta(x)+c\delta(x-\tilde{x})$ yields $a=c\tilde{x}/\pi$. The energy $e_4=c\tilde{x}^2/(2\pi^2)=a^2/(2c)$ is arbitrarily high for any given a when c is small.

B. Grand canonical distribution

The continuous entropy [15,16] related to $p(x)$ is

$$s[p(x)] = -\int_0^\infty p(x)\ln[hp(x)]dx. \tag{2}$$

The length scale h is set equal to 1. The entropy of the system of N oscillators is $S=Ns$. The equilibrium probability density yields the highest possible entropy. The density for the extremal entropy has to be determined with the constraints of fixed wave action, energy, and total probability $\int_0^\infty p(x)dx=1$. Using the Lagrange multipliers α, ϵ, and λ, this density is given by the extremum of the functional

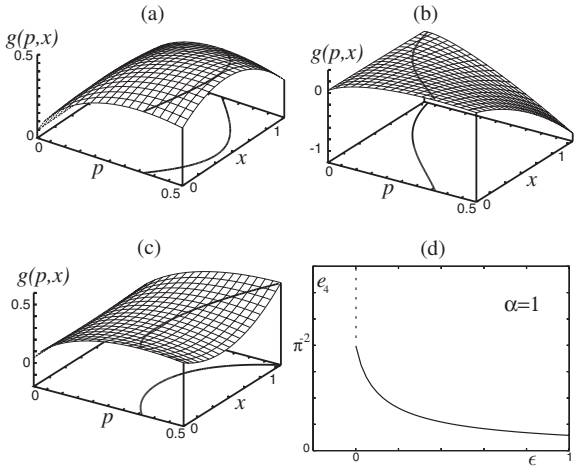

FIG. 3. The function $g(p,x)=-p\ln p-\alpha xp-\epsilon x^2p$ for different signs of the multipliers α and ϵ. (a) $\alpha=-1$, $\epsilon=1$ corresponding to domain I; (b) $\alpha=1$, $\epsilon=1$ corresponding to domain II; (c) $\alpha=1$, $\epsilon=-1$. The maximum $\partial g/\partial p=0$ yields the grand canonical distribution (line). The grand canonical distribution increases exponentially as a function of x for $\epsilon<0$. (d) The energy e_4 as a function of ϵ is finite for $\epsilon\geq 0$, and jumps to infinity at $\epsilon<0$.

$$G[p(x),x]=-\int_0^\infty p(x)\{\ln[p(x)]+\alpha x+\epsilon x^2+\lambda\}dx. \quad (3)$$

The extremum of $G[p(x),x]$ is given by

$$\int_0^\infty \delta p(x)\{\ln[p(x)]+1+\alpha x+\epsilon x^2+\lambda\}dx=0. \quad (4)$$

This is solved by the grand canonical probability distribution $p(x)=y^{-1}\exp(-\alpha x-\epsilon x^2)$. The partition function is $y=\int_0^\infty \exp(-\alpha x-\epsilon x^2)dx=\exp(1+\lambda)$. Figures 3(a)–3(c) show the integrand of Eq. (3) $g(p,x)=-p\ln p-\alpha xp-\epsilon x^2p$, for different signs of α and ϵ (the normalization parameter λ is skipped for simplicity). The grand canonical distribution follows the ridge $\partial g/\partial p=0$ of $g(p,x)$.

The lines $\alpha=0$ and $\epsilon=0$ split the range of possible energies $e_4\geq a^2/2$ into three domains, as shown in Fig. 2. The domains I and II are associated to the regime where no breathers emerge, while breathers do appear in domain III.

C. Regime with no breathers

In the domains I and II, the energy is within the band $a^2/2\leq e_4\leq a^2$ (Fig. 4). Equivalently, the second moment is confined by $\langle x\rangle^2\leq\langle x^2\rangle\leq 2\langle x\rangle^2$.

Domain I with $\alpha<0$, $\epsilon>0$ corresponds to low energies $a^2/2<e_4<\pi a^2/4$. Figure 3(a) shows that the density increases as a function of x at small x, but decays exponentially $p(x)\sim\exp(-\epsilon x^2)$ for large x.

Domain II with $\alpha>0$, $\epsilon>0$ matches the energy band $\pi a^2/4<e_4<a^2$. Figure 3(b) shows that the probability density decays exponentially as $p(x)\sim\exp(-\epsilon x^2)$ for high amplitudes x. This exponential decay of the probability makes high-amplitude peaks extremely unlikely. The border between the domains I and II corresponds to distributions with

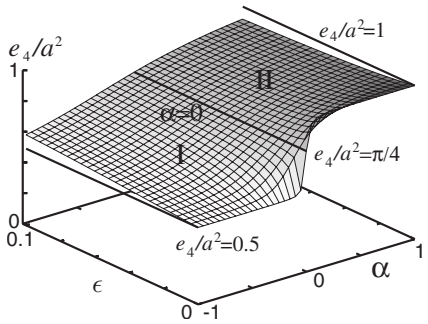

FIG. 4. The ratio $1/2<e_4/a^2<1$ for $\epsilon>0$. The line $\alpha=0$, $e_4/a^2=\pi/4$ separates domain I from domain II. For $\epsilon>0$ fixed and $\alpha\to\infty$, the energy converges to $e_4\to a^2$. For $\alpha\to-\infty$, it converges to the lower boundary $e_4\to a^2/2$. For $\epsilon\to\infty$ and α fixed, it converges to $e_4\to\pi a^2/4$.

$\alpha=0$, $\epsilon>0$. The extremum condition (4) is not constrained by a since the multiplier α is zero. The probability density is $p(x)=2\sqrt{\epsilon/\pi}\exp(-\epsilon x^2)$, which yields the relation of energy and wave action $e_4(a)=\pi a^2/4$. This distribution provides the highest entropy that can be achieved when e_4 is fixed. No other distribution with the same value of e_4 and with any value of a yields a higher entropy.

The probability is not constrained by the Hamiltonian when $\epsilon=0$ with $\alpha>0$. The probability distribution $p(x)=\alpha\exp(-\alpha x)$ is not a function of the Hamiltonian. This distribution is achieved on the line $e_4(a)=a^2$ (Fig. 2), which was first computed in [8]. The entropy at this line is $s=1+\ln(\pi a)$. No other distribution with the same wave action leads to a higher entropy.

D. Distribution in the regime with breathers

The line $\epsilon=0$ of Fig. 2 marks the transition to domain III where high-amplitude structures are found numerically. Domain III cannot be described by a grand canonical distribution: The grand canonical distribution $p(x)\sim\exp(-\alpha x-\epsilon x^2)$ increases exponentially at large x for $\epsilon<0$ [Fig. 3(c)]. The probability is gathered at infinite x. This leads to an infinite wave action a and energy e_4. Consequently, the energy $e_4(\epsilon)$ has a discontinuity at $\epsilon=0$ where it jumps from a finite value $e_4=a^2$ to an infinite value for $\epsilon<0$ [Fig. 3(d)].

The aim is now to find a distribution $p(x)$ that yields the maximum entropy for a finite energy within domain III. For this purpose the probability density is approximated by trial functions that have a finite first and second moment. The discontinuity [Fig. 3(d)] at $\epsilon=0$ disappears and the transition becomes smooth in this approximation. The approximation can be improved by increasing the number of trial functions. A discontinuity of the energy emerges again in the limit of an infinite number of trial functions.

With the ansatz $p(x)=q(x)\exp(-\alpha x-1-\lambda)$ the extremum of the functional (3) is given by

$$\int_0^\infty \delta p(x)[\ln q(x)+\epsilon x^2]dx=0. \quad (5)$$

The solution $q(x)\sim\exp(-\epsilon x^2)$ is ruled out, as it leads to the divergences of Fig. 3(c). A finite polynomial trial function

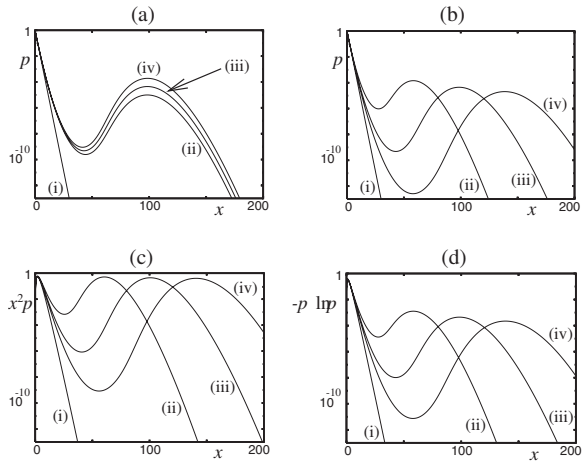

FIG. 5. (a),(b) Probability distribution $p(x)=q(x)\exp(-\alpha x-1-\lambda)$ with the approximation (6). (c) is the density $x^2p(x)$, (d) is the density of the entropy $-p(x)\ln p(x)$. The parameters for (a) are (i) $\epsilon=0$, (ii) $\epsilon=-0.0113$, (iii) $\epsilon=-0.011\,65$, (iv) $\epsilon=-0.012$, with $m=50$, $\alpha=1$. (b), (c), (d) show data for the parameters $\alpha=1$ and (i) $\epsilon=0$; (ii) $\epsilon=-0.018$, $m=30$; (iii) $\epsilon=-0.011\,65$, $m=50$; (iv) $\epsilon=-0.0086$, $m=70$.

$q(x)=\Sigma_{n=0}^{m}q_nx^{2n}$ ensures that energy and wave action are finite. The task is to choose coefficients q_n that yield the highest possible entropy for a finite energy and wave action within domain III.

The integrand of Eq. (5) is not close to zero for all x when $q(x)$ is a finite polynomial. For this reason certain variations $\delta p(x)$ have to be excluded from Eq. (5). The solution q_n depends on the variations $\delta p(x)$ that are admitted. In [17], the variation problem was solved with the Ritz method. The extremum of Eq. (3) with respect to q_n was computed numerically.

The finite exponential series approximation

$$q(x)=\sum_{n=0}^{m}(-\epsilon)^nx^{2n}/n! \tag{6}$$

with $\epsilon<0$ is used in the following. The justification for Eq. (6) is that it removes all powers up to x^{2m} from Eq. (5). The expression $\ln q(x)+\epsilon x^2$ with Eq. (6) is discussed in the Appendix for $-\epsilon$ small and m large. Figure 9(a) shows that this function is very small for $x<x_0=\sqrt{m/(-e\epsilon)}$ and grows as ϵx^2 for $x\gg x_0$ with (e is Euler's number).

Equation (6) solves Eq. (5) approximately when variations $\delta p(x)\neq 0$ are admitted only for $x<x_0$. The variations have to vanish $\delta p(x)=0$ for $x>x_0$. In other words, Eq. (6) yields a probability density that follows the rim of Fig. 3(c) for $x<x_0$. At very high x, $p(x)$ is below the rim. Figure 5(a) illustrates this probability density for various small $\epsilon<0$, and with $m=50$ and $\alpha=1$ fixed [lines (ii)–(iv)]. These probability densities are close to the canonical density [line (i)], but they have a small hump at $x\approx 2m=100$. The height of this hump increases when a larger value $-\epsilon$ is chosen.

The location $x\approx 2m$ of the hump depends on the order m of the polynomial (6). In Fig. 5(b), the parameters ϵ and m are changed in that way that humps $p(x=2m)\sim m^{-2}\sim x^{-2}$ are obtained [lines (ii)–(iv)]. The corresponding energy densities $x^2p(x)$ have humps of order 1 [Fig. 5(c)]. The densities (ii)–(iv) all yield $e_4=1$. For comparison, the density (i) with $\epsilon=0$ yields $e_4=\pi^{-2}$. This shows that the hump provides a substantial contribution to e_4. A formula that yields ϵ as a function of m, e_4, and a is derived in the Appendix. For m large,

$$\epsilon(m)=-\frac{e}{4\pi^2a^2}\left[m^{-1}+m^{-2}\ln\left((e_4/a^2-1)\frac{e-1}{\sqrt{8}em^2}\right)\right] \tag{7}$$

yields a finite energy $e_4>a^2$ within domain III (e is Euler's number). When m is finite, a finite energy corresponds to every finite $\epsilon<0$. Consequently, there is no jump discontinuity of e_4 at $\epsilon=0$.

$\epsilon(m)\to 0$ tends to zero in the limit $m\to\infty$. $e_4[m,\epsilon(m)]$ converges to a function with a finite jump at $\epsilon=0$. The energy at the transition is $e_4(\epsilon=0)=a^2$. At the limit from below, the energy can have any finite value $e_4[m\to\infty,\epsilon(m)\to 0^-]>a^2$. In the same limit, the range $x<x_0\sim m$ where variations $\delta p(x)\neq 0$ are admitted goes to infinity. In this range, the distribution converges to the canonical distribution $p(x)\sim\exp(-\alpha x)$. The hump $p(x=2m)\sim m^{-2}$ moves to infinity, and decays. So the hump has an infinitesimal probability, but a finite energy.

The contribution to the wave action and the entropy of the hump goes to zero in this limit. Figure 5(d) shows the density of entropy $-p(x)\ln p(x)$. The main contribution to the entropy is due to small x. The entropy density at the hump as a function of m decays $\sim m^{-2}\ln m$, which becomes negligible for m large.

Consequently, the entropy has the same value $s=1+\ln(\pi a)$ at the transition line $\epsilon=0$ and within domain III. The entropy as a function of the energy is continuous but not analytic at the transition. The entropy in domain III is independent of the energy, and depends only on a (Fig. 6).

To conclude this section, the probability distribution in domain III is almost the same as at the transition line $\epsilon=0$. It differs only by a tiny hump at a high amplitude [Fig. 5(a)]. This hump corresponds to the high-amplitude peaks that contain a part of the total energy. One may interpret the state in

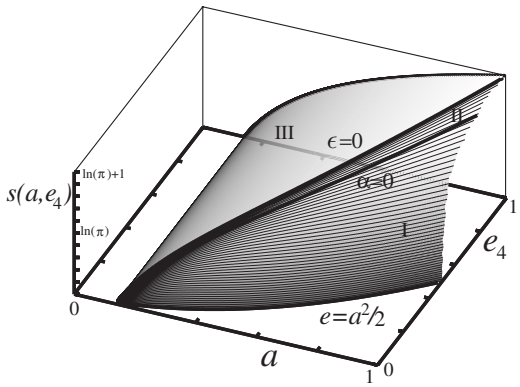

FIG. 6. Entropy per oscillator as a function of average wave action a and energy e_4 per oscillator. The entropy grows as a function of the energy e_4 in domains I and II. It reaches its maximum at the line $e_4=a^2$, where $\epsilon=0$. The entropy is independent of e_4 in domain III, where $s=1+\ln(\pi a)$.

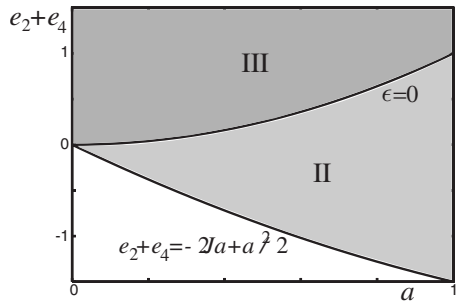

FIG. 7. Domain II with no breathers and domain III where breathers emerge. The domains are separated by the line $e_2+e_4=a^2$, where $\epsilon=0$. Domain II corresponds to $\alpha>0$, $\epsilon>0$. Domain I with $\alpha<0$ appears at higher values of a (compare Fig. 1 in Ref. [8]).

domain III as two "phases," one corresponding to the canonical density with $\epsilon=0$, $\alpha>0$, and one corresponding to the infinitesimal probability at an infinite amplitude. As there is a jump discontinuity of the energy $e_4(\epsilon)$ at $\epsilon=0$, the transition is similar to a first order phase transition. However, by $ds=\epsilon de_4$ there is no change of entropy when energy is added to the system, as the transition occurs at an infinite temperature ϵ^{-1}.

III. DISTRIBUTION FOR FINITE COUPLING

A. Transition behavior

The problem for the full Hamiltonian with a finite coupling strength $J\neq 0$ is studied in this section. The boundary conditions are periodic. It turns out that the results of the previous section can be applied to this case.

The coupling energy is $E_2=\Sigma_i 2\pi^{-1}\sqrt{x_i x_{i+1}}\cos\psi_i$ with the variables $x_i=\pi|\phi_i|^2$ and $\cos\psi_i=\mathrm{Re}(\phi_i\phi_{i+1}^*)/|\phi_i\phi_{i+1}^*|$. The energy per lattice site $e_2+e_4=E_2/N+E_4/N$ is bounded from below and unbounded from above. The state with the lowest energy per wave action is a wave with $\phi_{n+1}=-\phi_n$. The coupling energy of this wave is $E_2=-2JA$ and the quartic energy is $E_4=A^2/(2N)$. The energy per lattice site is $e_2+e_4=-2Ja+a^2/2$ (lower boundary in Fig. 7).

The highest energy at a given wave action is achieved for a peak $|\phi_l|\approx\sqrt{A}\gg 1$ that contains almost the whole wave action of the system. The amplitudes are very small at all other sites. This isolated peak has an energy $E_4\approx A^2/2$, while the coupling energy is negligible. The average energy per site $e_4\approx Na^2/2$ tends to infinity in the limit $N\to\infty$ with a fixed. The phase space volume element is $d\Gamma=(2\pi)^{-N}\Pi_i dx_i d\psi_i$. The task is again to find the probability distribution that yields the maximum entropy $S[p(x_1,\psi_1,\ldots,x_N,\psi_N)]=-(2\pi)^{-N}\int p\ln p\Pi_i dx_i d\psi_i$ for a given total energy and wave action. The variation problem $\delta[S-\alpha\pi A-\epsilon 2\pi^2(E_2+E_4)-\lambda\int p d\Gamma]=0$ is now extended by E_2.

The grand canonical distribution $p=\exp[-\alpha\pi A-\epsilon 2\pi^2(E_2+E_4)-1-\lambda]$ can again be applied to the regime with $\epsilon\geq 0$. Domain II in Fig. 7 corresponds to $\alpha>0$ and $\epsilon>0$. The probability distribution does not factorize in domain II. An explicit formula for the partition function and the entropy in the limit of small a was given in [10].

At a higher value of the wave action ($a=2J$ outside the range of Fig. 7, compare Fig. 1 in Ref. [8]) there is a transition $\alpha=0$ to domain I, where α is negative. Both in domains I and II, the probability density decays as $p\sim\exp(-\epsilon x^2)$ for high x. High-amplitude structures are extremely unlikely.

The transition line $\epsilon=0$, $\alpha>0$ is given by $e_2=0$, $e_4=a^2$ [8], which is the same as in the limit of weak coupling. The probability density factorizes as $p_N(x_1,\ldots,\psi_N)=\Pi_{i=1}^N p(x_i)$, with the same probability density $p(x_i)=\alpha\exp(-\alpha x_i)$ as in the limit of weak coupling. The distribution at $\epsilon=0$ is independent of the Hamiltonian, so the system achieves the highest entropy that is possible for this particular value of a.

B. Regime with breathers

High-amplitude breathers do appear for an energy $e_2+e_4>a^2$ in domain III (Fig. 7). The question is which probability distribution yields the maximum entropy within domain III. A grand canonical distribution with a negative temperature $\epsilon<0$ is ruled out since the probability density $p\sim\exp(-\epsilon 2\pi^2 E_4)$ diverges as a function of x.

As in Sec. II, this divergence can be avoided by constraining the probability distribution to a set of functions with a finite first and second moment. The ansatz for the probability density

$$p(x_1,\ldots,\psi_N)=\exp(-\alpha\pi A-\epsilon 2\pi^2 E_2-1-\lambda)\prod_i q(x_i,\epsilon) \tag{8}$$

removes A and E_2 from the variation. The variation now reads $\int_0^\infty\delta p\Sigma_i[\ln q(x_i)+\epsilon x_i^2]d\Gamma=0$. It reduces to Eq. (5) for each variable x_i, which can be solved approximately by the polynomial ansatz (6). The approximation can be improved by increasing m, while $\epsilon(m)$ tends to zero by Eq. (7).

The coupling factor $\exp(-2\pi^2\epsilon E_2)$ becomes negligible when ϵ goes to zero. It can be shown that

$$\begin{aligned}\exp(-\alpha\pi A) &< \exp(-\alpha\pi A)(2\pi)^{-N}\\ &\quad\times\int_0^{2\pi}\exp(-2\pi^2\epsilon E_2)\prod_i d\psi_i,\\ &< \exp[-(\alpha\pi+\epsilon 4\pi^2)A].\end{aligned} \tag{9}$$

Similarly, the energy contribution $E_2\sim O(\epsilon)$ vanishes. For $m\to\infty$, $\epsilon(m)\to 0^-$, the density reduces to $p(x_1,\ldots,x_N)=\Pi_i q(x_i)\exp(-\alpha x_i)$, which is the density for the weakly coupled case. The distribution is independent of the angles ψ_i.

As a result, in domain III the probability distribution factorizes into the same product for finite coupling and for weak coupling. In either case, the system contains two phases: One phase that comprises almost all oscillators, which absorb nearly the total wave action. The high amplitude phase has only an infinitesimal share of the probability and the wave action, but it contains a significant amount of energy.

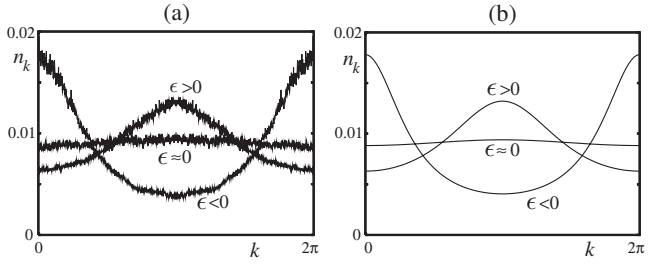

FIG. 8. (a) Numerical power spectra n_k averaged over 50 000 time units after an initial integration over 50 000 time units. The initial conditions are waves with $k=0$ ($\epsilon<0$), $k=0.55\pi$ ($\epsilon>0$), and $k\approx\pi/2$ ($\epsilon\approx0$) with $|\phi_n|=0.3$ and $J=1$. (b) Power spectra $n_k=(\alpha+\epsilon 2\cos k)^{-1}$ for $\alpha=2.4$, $\epsilon=0.425$; $\alpha=2.25$, $\epsilon=0.035$; $\alpha=3.1$, $\epsilon=-0.975$.

C. Comparison to numerical findings

The temperature ϵ^{-1} of low-amplitude waves can be measured by computing the power spectrum $n_k=\langle|a_k|^2\rangle$ with $a_k=N^{-1/2}\Sigma_n\phi_n\exp(-ikn)$. In equilibrium, a Rayleigh-Jeans distribution $n_k=(\epsilon\omega_k+\alpha)^{-1}$ is obtained. $\omega_k=2J\cos k$ is the frequency of linear waves of the discrete nonlinear Schrödinger equation. Figure 8(a) shows numerical spectra obtained from initial conditions $\phi_n=0.3\exp(ikn)$ plus weak noise. The system is first integrated over 50 000 time units so that it approaches its thermal equilibrium. The spectrum is computed by averaging over another 50 000 time units. The results can be compared to the matching Rayleigh-Jeans spectra of Fig. 8(b).

The initial condition with $k=0.55\pi$ yields a spectrum with $\epsilon>0$, corresponding to domain II. The initial condition with $k=\pi/2$ yields an almost flat spectrum with $\epsilon\approx0$. This is the same initial condition as for Fig. 1(b).

The spatially homogeneous initial condition $k=0$ corresponds to the simulation of Fig. 1(a). The energy $e_2+e_4=2a+a^2/2$ is within domain III. The spectrum shows that ϵ is negative. Another indication for a negative temperature was observed in Ref. [8]: In Fig. 1(a), $\ln p(x)$ has a slight curvature at small x. At $\epsilon=0$, it is a straight line [Fig. 1(b)]. The observation of this change of the curvature at the transition was discussed in detail in [11].

The finding of a negative temperature of the low-amplitude waves in domain III is somewhat surprising, as the equilibrium state corresponds to $\epsilon=0$. In other words, the system has not yet reached the equilibrium. One would expect that the breathers continue to grow or to merge into a smaller number of peaks with a higher amplitude. This would allow the low-amplitude phase to achieve a flat spectrum and a canonical distribution $p(x)\sim\exp(-\alpha x)$ that corresponds to the maximum of entropy.

However, the numerically observed peaks with the height $|\phi|^2\approx4.5$ are extremely stable. They do not move and merge into a smaller number of higher peaks in long-time numerical integrations.

Three mechanisms appear to stop the process of growth and merging of breathers. First, breathers of a critical amplitude near $|\phi|=2$ are pinned at the lattice [18]. The breathers cannot move and merge into a larger breathers.

Second, the interaction of peaks and low-amplitude waves becomes very weak when the peaks reach a critical height [19]. This is due to the disappearance of low-order interactions of waves and high-amplitude breathers. The height computed in [19] corresponds approximately to the maximum height of breathers in numerical experiments.

Finally, there is a statistical effect that breathers grow only if their nonlinear phase frequency is above the chemical potential of the surrounding waves [20]. This explains why no new breathers emerge from the disordered waves in the space between the breathers of [Fig. 1(a)].

IV. CONCLUSIONS

To summarize, the transition between the disordered low-amplitude regime [Fig. 1(b)] and the regime of high-amplitude structures [Fig. 1(a)] was studied. The type of behavior depends on the system's two conserved quantities, the wave action and the energy.

No high amplitude structures emerge if the energy per lattice site is below the threshold $e_2+e_4\leq a^2$ (Fig. 7). The distribution in this regime is grand canonical, and the probability for high-amplitude excitations decays exponentially.

At the transition line $e_2+e_4=a^2$, the distribution is independent of the Hamiltonian since the multiplier ϵ is zero. The probability factorizes into a product of the distributions of single oscillators. The phase differences ψ_n of neighboring oscillators are randomly and equally distributed, and the power spectrum in wave number space is white (Fig. 8). The amplitude of the oscillators is distributed canonically $p(|\phi|^2)\sim\exp(-\alpha|\phi|^2)$ so that no high-amplitude peaks appear [Fig. 1(b)].

High-amplitude breathers appear at $e_2+e_4>a^2$ in domain III above the transition $\epsilon=0$. The probability distribution was computed from the condition of an extremal entropy. The probability distribution was constrained to a set of ansatz functions that yield finite moments for $\epsilon<0$.

The probability distribution in the regime of breathers is most similar to that at the transition line $\epsilon=0$: The only difference is an infinitesimal augmentation of the probability $p(\phi)$ at infinite amplitudes $|\phi|$. This reflects the formation of a few structures with a very high amplitude, similar to the observation in Fig. 1(a). This high-amplitude phase at a few lattice sites contains a significant part of the total energy. The oscillators have a low amplitude with the same distribution as for $\epsilon=0$ at almost all lattice sites. This low-amplitude phase yields the system's total amount of entropy and wave action, and a part of the energy. The entropy is independent of the energy in the regime of breathers (domain III in Fig. 7). The entropy as a function of the energy is continuous but not analytic at the transition.

The nature of the transition can be understood from the weakly coupled system of Sec. II. As the sample space reduces to one dimension, the probability density yields the extremal entropy $s(\langle x\rangle,\langle x^2\rangle)=-\int_0^\infty p(x)\ln p(x)dx$ as a function of the first and the second moment. The distribution is grand canonical only for $\langle x^2\rangle\leq2\langle x\rangle^2$. For $\langle x^2\rangle$ larger, the distribution is almost canonical, but has an infinitesimally increased probability for an infinite amplitude. The constraint of a large

second moment $\langle x^2\rangle > 2\langle x\rangle^2$ leads to the formation of a high-amplitude phase. The first two moments correspond to A and E_4. The coupling part E_2 of the Hamiltonian with $J \neq 0$ has no influence on the probability distribution at the transition and within the breather regime, since ϵ vanishes. The transition is not caused by the coupling, and it exists also for weak coupling as well as in higher dimensional lattices.

APPENDIX

1. Variation at moderate amplitudes

The expression $\ln q(x) + \epsilon x^2$ of Eq. (5) is discussed for $x < x_0$ and for $x > x_0$, with $x_0 = \sqrt{(-m/(e\epsilon))}$, $0 < -\epsilon \ll 1$, $m \gg 1$, $-\epsilon \sim O(1/m)$. $x < x_0$: The polynomial (6) can be written as

$$q(x) = \exp(-\epsilon x^2) - \sum_{n=m+1}^{\infty} (-\epsilon)^n x^{2n}/n!. \tag{A1}$$

Multiplying this expression by $\exp(\epsilon x^2)$ and taking the logarithm yields

$$\epsilon x^2 + \ln q(x) = \ln\left(1 - \exp(\epsilon x^2) \sum_{n=m+1}^{\infty} (-\epsilon x^2)^n/n!\right). \tag{A2}$$

The Stirling formula yields the approximation $(-\epsilon x^2)^n/n! \approx (-\epsilon e x^2/n)^n/\sqrt{2\pi n}$. The sum in Eq. (A2) can be estimated as

$$\begin{aligned}\sum_{n=m+1}^{\infty} (-\epsilon x^2)^n/n! &\approx \sum_{n=m+1}^{\infty} (-\epsilon e x^2/n)^n/\sqrt{2\pi n} \\ &< (2\pi m)^{-1/2} \sum_{n=m+1}^{\infty} (x/x_0)^{2n} \\ &= \frac{(x/x_0)^{2m+2}}{\sqrt{2\pi m}[1-(x/x_0)^2]}.\end{aligned} \tag{A3}$$

For $x < x_0$, this expression becomes small for m large. With $\exp(\epsilon x^2) \leq 1$, the argument in the logarithm in Eq. (A2) approaches one when m is large, so Eq. (A2) goes to zero.

$x \gg x_0$: Replacing the polynomial $q(x)$ by its highest order term yields $\ln q(x) \sim m \ln(x^2/x_0^2)$. This is small compared to $-\epsilon x^2 = m x^2/(e x_0^2)$, so Eq. (A2) yields $\ln q(x) + \epsilon x^2 \approx \epsilon x^2$ in the limit of high x.

For this reason only variations $\delta p(x)$ are admitted that are zero for $x > x_0$ [Fig. 9(a)]. This choice of variations keeps the integrand of $\delta G = \int_0^\infty \delta p(x)[\epsilon x^2 + \ln q(x)]dx$ equal to zero. The region $x < x_0$ where variations are admitted can be extended arbitrarily by choosing a smaller parameter $-\epsilon$. The tail $x_0 < x < \infty$ yields only a negligible contribution to the entropy since $p(x)$ is very small in this regime.

2. Relationship of ϵ and m

The probability density (5) and (6) yields an energy e_4 that depends on the Lagrange-parameter ϵ, and on the order m of the polynomial (6). It is shown that the relation (7)

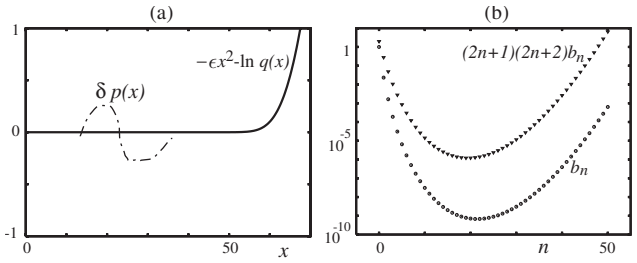

FIG. 9. (a) $-\epsilon x^2 - \ln q(x)$ is very small for $x < \sqrt{-m/(e\epsilon)}$, and increases quadratically at higher x. Variations $\delta p(x)$ in the range $x < \sqrt{-m/(e\epsilon)}$ yield only a negligible contribution to $\int \delta p(x)[\epsilon x^2 + \ln q(x)]dx$. (b) b_n and $(2n+1)(2n+2)b_n$ over n. $m=50$, $e_4=1$, $\alpha = 1$, $\epsilon = -0.011\,65$.

yields a fixed finite energy when m is large. The partition function $y = \int_0^\infty \exp(-\alpha x) q(x) dx$ for the ansatz (6) is

$$y_m = \int_0^\infty \exp(-\alpha x) \sum_{n=0}^{m} (-\epsilon)^n x^{2n}/n\,!\,dx = \alpha^{-1} \sum_{n=0}^{m} b_n \tag{A4}$$

with $b_n = (-\epsilon\alpha^{-2})^n (2n)\,!\,/n!$. Figure 9(b) shows the summands b_n over n for $0 < -\epsilon \ll 1$: At low n, b_n decays rapidly due to the factor $(-\epsilon\alpha^{-2})^n$. At higher n, the rapidly growing factor $(2n)\,!\,/n!$ prevails and b_n grows. For n large, the Stirling approximation $n! \approx \left(\frac{n}{e}\right)^n \sqrt{2\pi n}$, yields $b_n \approx \sqrt{2}(\gamma n)^n$ with $\gamma = -4\epsilon/(e\alpha^2)$, and Euler's number e. Equivalently, the sequence b_n evolves by the rule

$$\begin{aligned} b_{n+1} &\approx \sqrt{2}[\gamma(n+1)]^{n+1} = \sqrt{2}(\gamma n)^n [\gamma n(1+1/n)](1+1/n)^n \\ &\approx b_n \gamma n e. \end{aligned} \tag{A5}$$

b_n has its minimum at $n \approx (e\gamma)^{-1}$. b_n grows increasingly rapidly for $n > (e\gamma)^{-1}$ and reaches its maximum at $n = m$.

The partition function (A4) has major contributions only from its two maxima at $n=0$ and at $n=m$. At the lower end, $b_1 \sim O(\epsilon)$ is already negligibly small compared to $b_0 = 1$. At the upper end, the summands near $n=m$ in Eq. (A4) can be added up as

$$\begin{aligned} b_m + b_{m-1} + b_{m-2} + \ldots &\approx \sqrt{2}(\gamma m)^m [1 + (\gamma m e)^{-1} + (\gamma m e)^{-2} + \ldots] \\ &\approx \sqrt{2}(\gamma m)^m \gamma m e/(\gamma m e - 1). \end{aligned} \tag{A6}$$

The partition function is

$$y_m \approx \alpha^{-1}[1 + \sqrt{2}(\gamma m)^m \gamma m e/(\gamma m e - 1)] \tag{A7}$$

where only b_0 and the highest summands of Eq. (A4) are considered. Similarly, the second moment is computed as

$$\begin{aligned} \langle x^2 \rangle &= y_m^{-1} \int_0^\infty x^2 \exp(-\alpha x) \\ &\quad \times \sum_{n=0}^{m} \frac{(-\epsilon x^2)^n}{n!} dx = y_m^{-1} \alpha^{-3} \sum_{n=0}^{m} (2n+1)(2n+2) b_n \\ &\approx y_m^{-1} \alpha^{-3} [2b_0 + 4m^2 (b_m + b_{m-1} + \ldots)] \end{aligned}$$

$$\approx y_m^{-1}\alpha^{-3}\left(2+4m^2\sqrt{2}(\gamma m)^m\frac{\gamma me}{\gamma me-1}\right), \tag{A8}$$

where $b_0=1$ and the approximations (A6) and $(2n+1)(2n+2)\approx 4m^2$ for $n\approx m\gg 1$ are applied.

For $\epsilon=0$ or equivalently $\gamma=0$, b_0 is the only contribution to Eqs. (A4) and (A6). The second moment is $\langle x^2\rangle = 2y^{-1}\alpha^{-3}=2\alpha^{-2}$.

For $\gamma=m^{-1}$, Eq. (A8) is dominated by the summands near $n=m$. This yields the very large second moment $\langle x^2\rangle = y_m^{-1}\alpha^{-3}[2+4m^2\sqrt{2}e/(e-1)]\sim O(m^2)$.

For some γ slightly smaller than m^{-1} it can be achieved that $(\gamma m)^m\sim O(m^{-2})$. This yields contributions of the same order from the first and the second term in Eq. (A8). The partition function is $y_m\approx\alpha^{-1}$ in this case, since the second term $(\gamma m)^m\sim O(m^{-2})$ in Eq. (A7) is negligibly small. With $\langle x^2\rangle=2\pi^2 e_4$, Eq. (A8) can be written as

$$2\pi^2 e_4\approx\alpha^{-2}\left(2+4m^2\sqrt{2}(\gamma m)^m\frac{\gamma me}{\gamma me-1}\right). \tag{A9}$$

This is solved approximately by

$$\gamma = m^{-1}+m^{-2}\ln\frac{(1-e)(1-\pi^2\alpha^2 e_4)}{\sqrt{8}em^2}, \tag{A10}$$

or $\epsilon(m)$ of Eq. (7). Again, this shows that ϵ becomes small for large m. For the first moment

$$\begin{aligned}\langle x\rangle &= y_m^{-1}\int_0^\infty x p_m(x)dx\\ &= y_m^{-1}\alpha^{-2}\sum_{n=0}^{m}(2n+1)b_n\\ &\approx y_m^{-1}\alpha^{-2}[1+2m\sqrt{2}(\gamma m)^m\gamma me/(\gamma me-1)],\end{aligned} \tag{A11}$$

the second term $m(\gamma m)^m\sim O(m^{-1})$ is negligible. This yields $a=\langle x\rangle/\pi\approx\alpha^{-1}\pi^{-1}$.

[1] M. Sato, B. E. Hubbard, A. J. Sievers, B. Ilic, D. A. Czaplewski, and H. G. Craighead, Phys. Rev. Lett. **90**, 044102 (2003).
[2] P. Binder, D. Abraimov, A. V. Ustinov, S. Flach, and Y. Zolotaryuk, Phys. Rev. Lett. **84**, 745 (2000).
[3] M. Peyrard, Nonlinearity **17**, R1 (2004).
[4] B. I. Swanson, J. A. Brozik, S. P. Love, G. F. Strouse, A. P. Shreve, A. R. Bishop, W. Z. Wang, and M. I. Salkola, Phys. Rev. Lett. **82**, 3288 (1999).
[5] U. T. Schwarz, L. Q. English, and A. J. Sievers, Phys. Rev. Lett. **83**, 223 (1999).
[6] A. A. Sukhorukov, Y. S. Kivshar, H. S. Eisenberg, and Y. Silberberg, IEEE J. Quantum Electron. **39**, 31 (2003).
[7] Th. Anker, M. Albiez, R. Gati, S. Hunsmann, B. Eiermann, A. Trombettoni, and M. K. Oberthaler, Phys. Rev. Lett. **94**, 020403 (2005).
[8] K. O. Rasmussen, T. Cretegny, P. G. Kevrekidis, and N. Gronbech-Jensen, Phys. Rev. Lett. **84**, 3740 (2000).
[9] B. Rumpf and A. C. Newell, Phys. Rev. Lett. **87**, 054102 (2001); Physica D **184**, 162 (2003).
[10] B. Rumpf, Phys. Rev. E **69**, 016618 (2004).
[11] M. Johansson and K. O. Rasmussen, Phys. Rev. E **70**, 066610 (2004).
[12] J. L. Lebowitz, H. A. Rose, and E. Speer, J. Stat. Phys. **50**, 657 (1988); **54**, 17 (1989).
[13] B. Rider, J. Stat. Phys. **113**, 575 (2003).
[14] B. Jordan, B. Turkington, and C. L. Zirbel, Physica D **137**, 353 (2000).
[15] A. Hobson and B.-K. Cheng, J. Stat. Phys. **7**, 301 (1973).
[16] E. T. Jaynes, Phys. Rev. **106**, 620 (1957).
[17] B. Rumpf, Phys. Lett. A **372**, 1579 (2008).
[18] Y. S. Kivshar and D. K. Campbell, Phys. Rev. E **48**, 3077 (1993); B. Rumpf, *ibid.* **70**, 016609 (2004).
[19] M. Johansson and S. Aubry, Phys. Rev. E **61**, 5864 (2000); M. Johansson, *ibid.* **63**, 037601 (2001).
[20] B. Rumpf, Europhys. Lett. **78**, 26001 (2007).